Fractured-karst spring-flow protections: a case study in Jinan, China

Jiazhong Qian · Hongbin Zhan · Yifeng Wu · Fulin Li · Jiaquan Wang

Abstract Jinan Springs are an important historical heritage in China and have been well known for hundreds of years. Over-abstraction of groundwater in the Jinan area has seriously endangered the hydrological system of the springs, which have stopped flowing for significant periods of time in recent years. A three-dimensional finite-element model programmed primarily at the Hefei University of Technology has been developed to simulate groundwater level change in the large fractured-karst aquifer system in the Jinan Springs field. Various spring protection plans have been explored and their effects on the water table analyzed and compared. It was found that the present rate of groundwater withdrawal from the fractured-karst system in this area was inappropriate for spring protection. The simulated results suggest that decreasing the rate of groundwater pumping from 6.9×10^5 to 2.7×10^5 m^3/day is needed to protect spring flows. Additional water resource requirements in that area may be met by use of surface water and recycled waste water.

Résumé Les sources de Jinan représentent un héritage historique important en Chine et sont bien connues depuis des centaines d'années. La surexploitation des eaux souterraines dans la région de Jinan a considérablement affecté le système hydrologique des sources ; celles-ci se sont taries pendant des durées importantes ces dernières années. Un modèle aux éléments finis en trois dimensions, programmé à l'origine à l'Université de la Technologie de Hefei, a été réalisé pour simuler le changement du niveau de l'eau souterraine dans le grand système aquifère karstique fracturé de la région des sources de Jinan. Divers plans de protection des sources ont été envisagés et leurs effets sur l'aquifère ont été analysés et comparés. Le taux actuel de prélèvement d'eau souterraine à partir du système karstique fracturé s'est avéré comme étant incompatible avec la protection des sources. D'après les résultats des simulations, une diminution du taux de pompage des eaux souterraines de 6.9×10^5 à 2.7×10^5 m^3/j est nécessaire pour sauvegarder l'écoulement des sources. Dans cette région, l'utilisation de l'eau de surface et le recyclage des eaux usées devraient permettre de satisfaire la demande en eau supplémentaire.

Resumen Los manantiales Jinan son un importante patrimonio cultural en China y han sido bien conocidos por cientos de años. La sobre utilización de agua subterránea en el área Jinan ha amenazado seriamente el sistema hidrológico de los manantiales los cuales han dejado de fluir durante periodos significativos de tiempo en años recientes. Se ha desarrollado un modelo tridimensional en elemento finito programado principalmente en la Universidad Tecnológica de Hefei para simular el cambio de nivel de agua subterránea en el sistema de acuífero kárstico fracturado del campo de manantiales Jinan. Se han explorado varios planes de protección de manantiales y se han comparado y analizado sus efectos en el nivel freático. Se encontró que la tasa actual de explotación de agua subterránea en el sistema kárstico fracturado del área ha sido inadecuada para la protección de los manantiales. Los resultados de simulación sugieren que es necesario disminuir el bombeo de agua subterránea de 6.9×10^5 a 2.7×10^5 m^3/d para proteger los flujos de los manantiales. Los requerimientos adicionales de recursos hídricos en el área pueden ser abastecidos con el uso de agua superficial y agua residual reciclada.

Keywords Three-dimensional model · Karst · Groundwater flow · Spring protection · Jinan Springs

Received: 7 September 2004 / Accepted: 5 May 2006
Published online: 15 September 2006

J. Qian · Y. Wu · J. Wang
School of Natural Resources and Environmental Engineering,
Hefei University of Technology,
Hefei, 230009, People's Republic of China

H. Zhan (✉)
Department of Geology and Geophysics,
Texas A and M University,
College Station, TX 77843-3115, USA
e-mail: zhan@geo.tamu.edu
Tel.: +1-979-8627961
Fax: +1-979-8456162

F. Li
Water Conservancy Research Institute of Shandong Province,
Jinan, 250013, People's Republic of China

 DOI 10.1007/s10040-006-0061-0

Introduction

Jinan is an important industrial and recreational city in Shandong province of China. It has been well known for its fractured-karst springs for hundreds, if not thousands of years. With rapid economic development and expansion of the city in the last 20 years, the rate of groundwater withdrawal from the local fractured-karst system has increased to a value that significantly lowered the water table. This in turn seriously affects the hydrological cycle of the spring system. Some of the springs that have discharged water for hundreds of years were first reported as having recently stopped flowing (Li et al. 2003). Such a consequence has not only damaged the recreational industry of the area, but also impacted the normal functionality of the city. Studying ground water flow in the fractured-karst springs system is vital for wisely managing the precious groundwater resources in the region. Similar problems related to fractured-karst springs can be found in many other countries such as France (Labat et al. 2002), Germany (Birk et al. 2004), Greece (Crouch 1996), Iran (Raeisi and Karami 1996), Italy (Sauro 1993), Romania (Oraseanu and Mather 2000), Syria (Kattan 1997), Turkey (Elhatip and Gunay 1998), and United States (Scanlon et al. 2003).

A numerical model has been selected to study groundwater flow in the fractured-karst media in Jinan and its result will be used to guide the spring protection strategy. Because of the difficulty to evaluate the distribution and geometry of fractures in a karst aquifer, an equivalent porous media model (EPMM) is often used to simulate a fractured-karst aquifer (Kaufmann and Braun 2000; Kaufmann 2003). For example, Scanlon et al. (2003) has proven the validity of EPMM for simulating regional groundwater flow in a karst system in Texas, USA. Josnin et al. (2000) has applied EPMM to a karst system in Saint-Chaptes Basin, France. Several studies in China have shown that many large fractured-karst aquifers often approximately follow Darcy's law, regardless of the uneven distribution of the fractures and karst networks (Wang and Zhang 1999; Wu et al. 1999; Zhu et al. 2000; Chen and Zhang 2001; Qian et al. 2003). Larocque et al. (1999) has provided a method of determining the equivalent permeability of a karst aquifer using EPMM. However, it is important to note that EPMM is a simplification of realistic fractured-karst systems which are often too complex to deal with precisely. For a large-scale flow scenario such as this study (see Fig. 1a), treatment of a fractured-karst medium as homogeneous might lead to a reasonably good agreement with an equivalent porous medium. However, for some cases, when preferential fracture and/or channel flows appear to be dominant, EPMM might not be appropriate and a different approach such as a discrete network model might be adopted (Jaquet et al. 2004). Nevertheless, EPMM was used in this study.

A three-dimensional finite-element model provides an efficient scheme for describing the irregular space and boundary of hydrogeologic systems and surface water bodies. In this study, a three-dimensional finite-element scheme was used to simulate the behavior of groundwater under various exploitation scenarios, to try to find an optimal plan to resolve the conflict of water supply and spring protection.

Description of the study area

Geography and geology of the study area

Figure 1a and b show the geographical location and the geological setting of the Jinan Springs field which covers more than 2,614 km^2 north of Tai Mountain in Shandong province of China. The eastern and western boundaries are Dongwu and Mashan faults, respectively. The southern boundary is the water divide of Chang Cheng Ling, and the northern boundary is the bared/concealed intrusive rocks along the Xiaoqinghe River. The southern part of the study area is a mountainous region with an average elevation of 500 meters above the sea level (m a.s.l.). The northern part of the study area is an alluvial flood plain with an average elevation of 28 m a.s.l. The city of Jinan is located at the conjunction of the mountain and the flood plain (Fig. 1b).

Geological data show that the tectonic unit in the Jinan Springs field belongs to the northern edge of doming structure in Tai Mountain, the northern wing of the Lu Zhongnan anticline. There are a variety of geological layers in the area, including Archaean layer (Ar), Cambrian (∈), Ordovician (O), Quaternary (Q), and the igneous rock (γ). There are many active faults in the spring field. The faults, such as Wenzu, Dongwu, Qianfoshan, Chaomidian, Mashan, and Ganggou faults, are aligned approximately along the north–south direction.

Hydrogeological conditions

The natural groundwater system consists of multi-layered units with various thicknesses and hydraulic properties. The main hydrogeological units in Jinan Springs field are: (1) Cambrian aquifer (∈), (2) Ordovician aquifer (O), (3) Quaternary aquifer (Q), and (4) Archaean aquifer (Ar). Groundwater flow is controlled by the characteristics of the aquifers and confining layers. It is also affected by the surface water (e.g., the surface reservoir, river, etc.), as well as the pumping and recharge wells.

The hydrogeological conditions are complex mainly due to the various layers and faults. The spring field is recharged by precipitation, mainly in the areas with bared layers of ∈ and O from the mountain in the south. The leakage of rivers such as Yufuhe and Beisha rivers and the reservoir such as Wohushan reservoir and the lateral inflow also contribute a great deal to groundwater recharge (Fig. 1a and b). In addition, the lower fractured-

 DOI 10.1007/s10040-006-0061-0

a

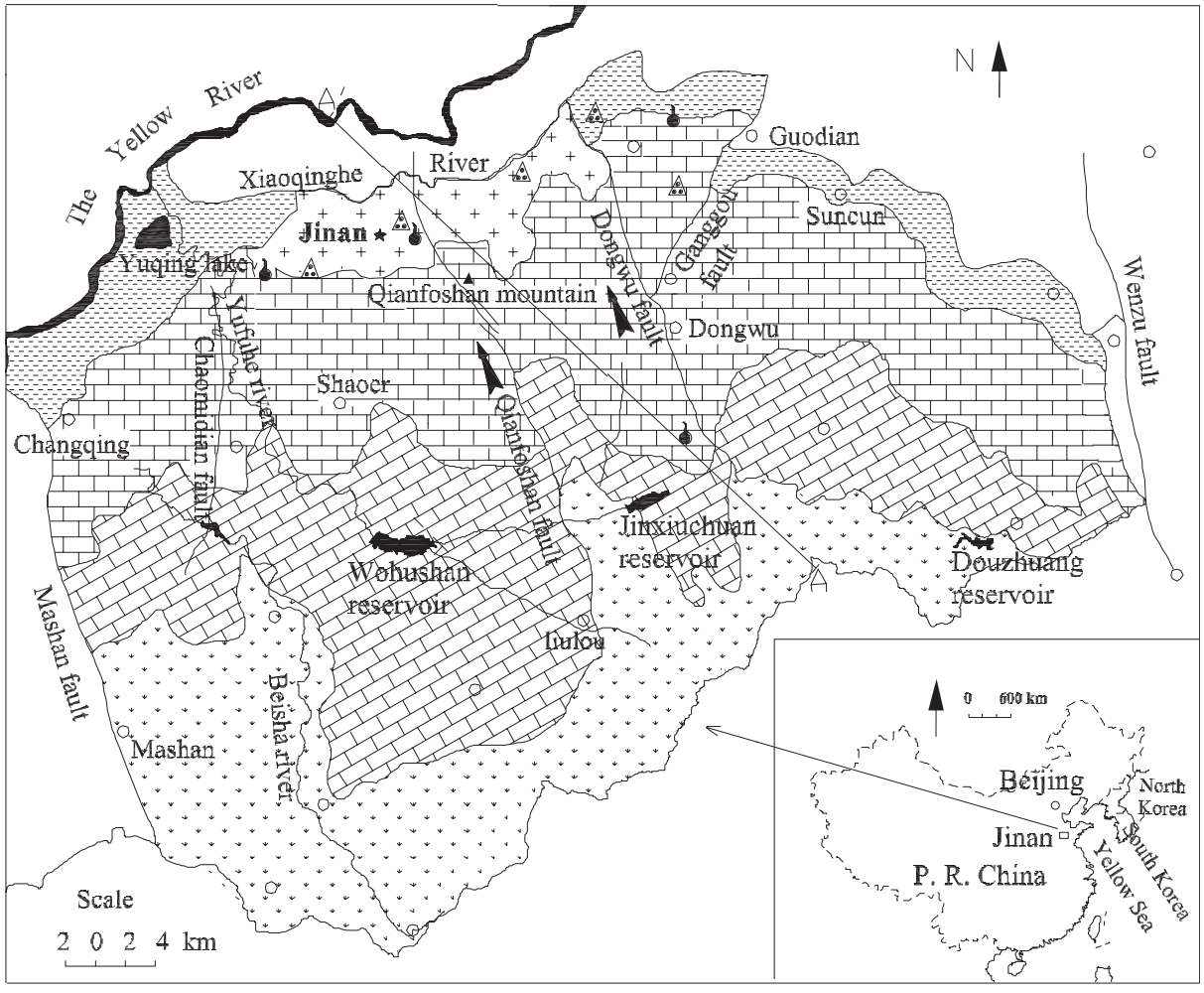

b

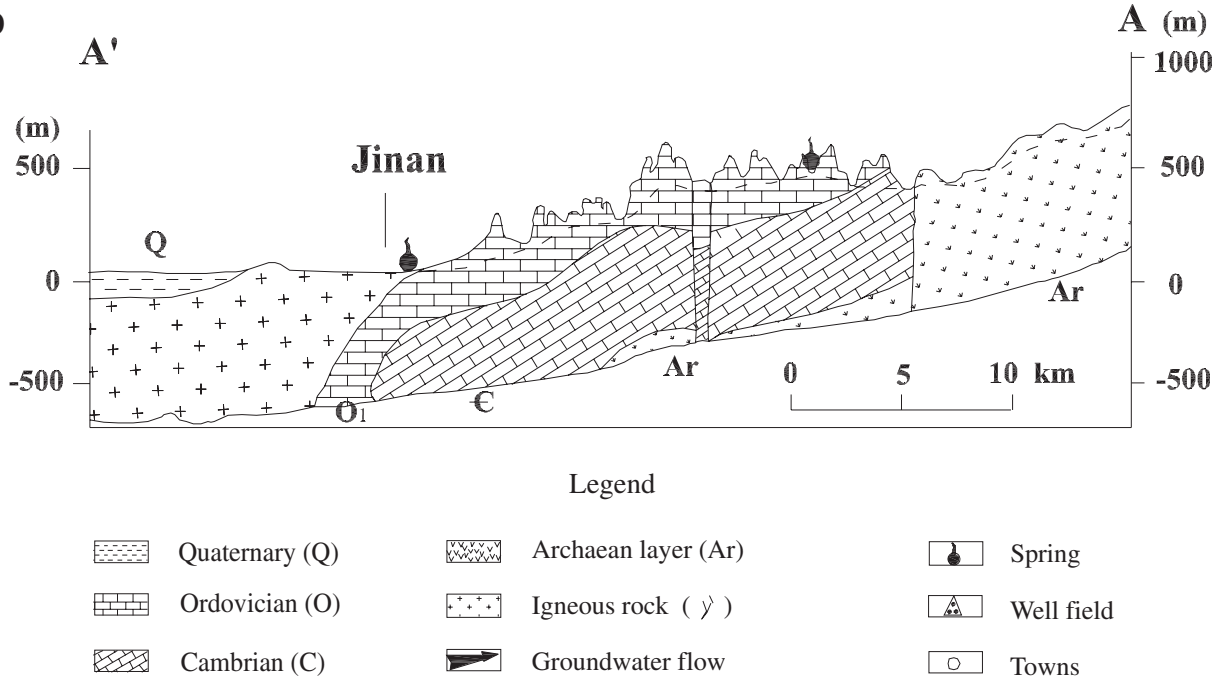

 DOI 10.1007/s10040-006-0061-0

karst aquifer system is recharged by the leakage from the upper Quaternary aquifer. Groundwater flow is generally from southeast to northwest and is controlled by the topography and faults. Limited by the igneous rocks in the north, groundwater flows upward when approaching the north. Under natural flow conditions, the upward flow finally discharges to the ground surface and forms the well-known Jinan spring series such as the Baotu Spring, the Black-Tiger Spring, the Pearl Spring, and the Five Dragon Spring (the four big springs). However, with the development of industry and agriculture, and urbanization of Jinan, groundwater exploitation becomes the main form of aquifer discharge. Therefore, the flow rates from the springs have declined considerately and some springs have become dry. According to the historical data, the Baotu Spring was dry all year round in 1982, 1989, and 2000. Furthermore, being dry from 2 March 1999 to 17 September 2001 for a total of 926 days, it has had the longest dry period in the history of the four big springs (Li et al. 2003). Spring protection in this area has become an urgent problem for sustainable development.

The Jinan spring series are the surface discharge points of the subsurface fractured-karst aquifers, similar to what has been found in the springs of the Edwards Aquifer in southern Texas, USA (Scanlon et al. 2003). These springs appear to be well connected with the aquifers without hydraulic barriers. Based on the geological and hydrogeological data of the region, a three-dimension transient flow model is presented in the following.

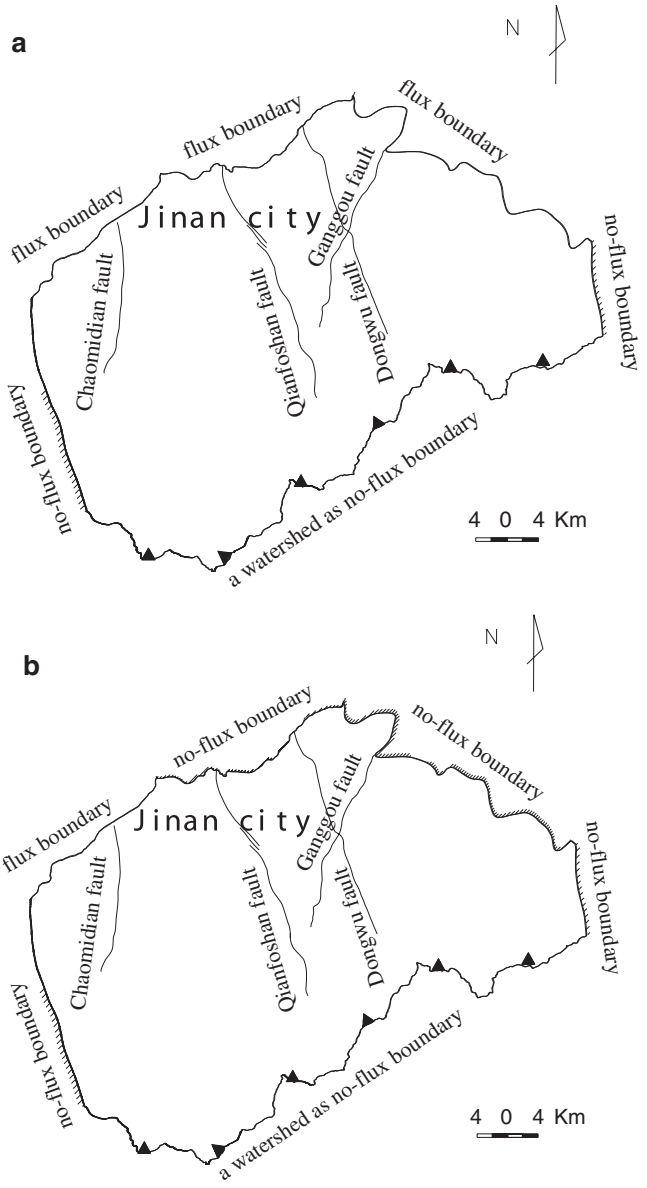

Fig. 2 The boundary conditions for **a** the first layer, and **b** the second and third layers. The *black triangle* indicates water divide that is treated as a no-flow boundary

Conceptual and mathematical models

Governing equation

The three-dimensional transient flow model is expressed as

$$\begin{cases} \dfrac{\partial}{\partial x}\left(K_{xx}\dfrac{\partial H}{\partial x}\right)+\dfrac{\partial}{\partial y}\left(K_{yy}\dfrac{\partial H}{\partial y}\right)+\dfrac{\partial}{\partial z}\left(K_{zz}\dfrac{\partial H}{\partial z}\right)+W=S_s\dfrac{\partial H}{\partial t},(x,y,z)\in\Omega \\ H(x,y,z,0)=H_0(x,y,z), \\ H(x,y,z,t)=\varphi(x,y,z,t),(x,y,z)\in s_1 \\ K_{xx}\cos(\mathbf{n},x)\dfrac{\partial H}{\partial x}+K_{yy}\cos(\mathbf{n},y)\dfrac{\partial H}{\partial y}+K_{zz}\cos(\mathbf{n},z)\dfrac{\partial H}{\partial z}=q,(x,y,z)\in s_2 \end{cases} \quad (1)$$

◀ **Fig. 1** **a** The geographical location and the hydrogeological map of the Jinan Springs field in Shandong province, China; **b** Geological profile of the Jinan Springs field. The *dashed line* represents the water table

where K_{xx}, K_{yy}, K_{zz} are the saturated hydraulic conductivities along the x, y, and z-axes, respectively; H (x, y, z, t) is the hydraulic head; H_0 (x, y, z) is the initial head; t is time; S_s is the specific storage; $W=W_p+W_s+W_r-W_e-Q$, where W_p, W_s, W_r, W_e, Q are the precipitation, the recharge by irrigation, the

 DOI 10.1007/s10040-006-0061-0

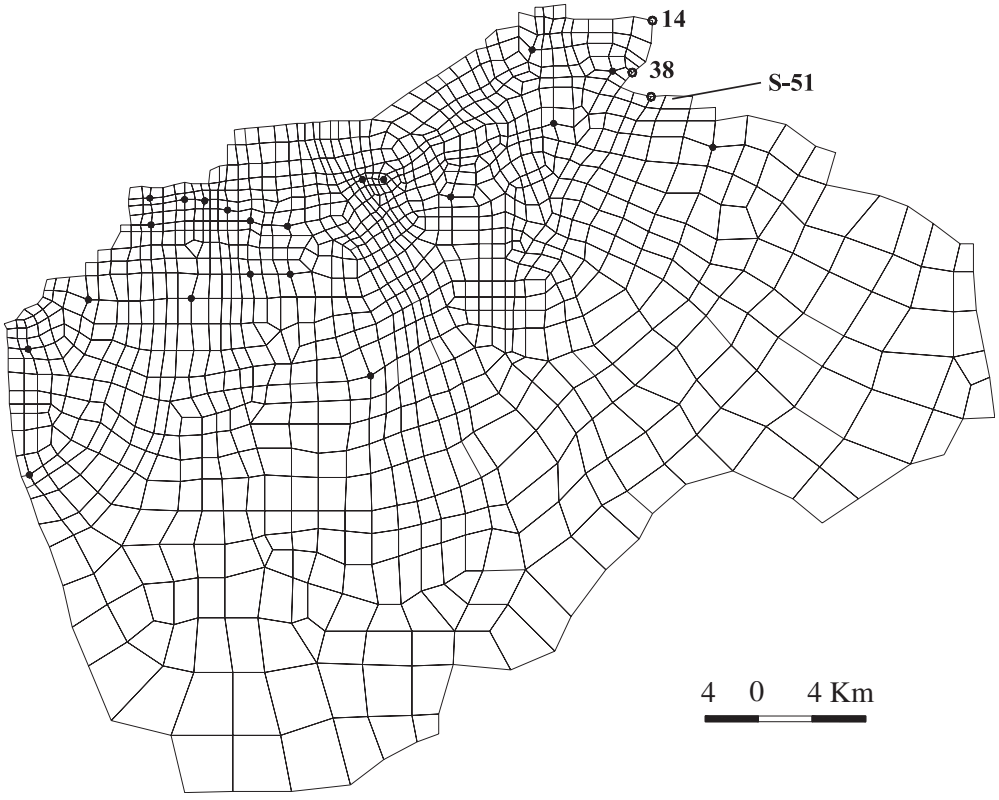

Fig. 3 The mesh of discretization. The *black point*s stand for the observation wells screened in the second layer. Wells numbered 14, 38, and S-51 are used for the first type of boundary condition

recharge by seepage from reservoirs, the evapotranspiration, and the well discharge from the aquifer, respectively; Ω is the study domain, s_1 and s_2 represent the first kind (Dirichlet) and the second kind (Neumann) boundary conditions, respectively; ϕ (x, y, z, t) is the head along the first kind boundary; **n** is the unit vector along the normal direction of the second kind boundary; cos(**n**, x), cos(**n**, y), and cos(**n**, z) are the angles between **n** and the x, y, and z directions, respectively; and q is the specific discharge across the second kind boundary.

Boundary conditions

Based on the geological characteristics of the site, a three-layer hydro-stratigraphic conceptual model is chosen to approximate the aquifer. Some topographic variations can be seen from the cross-section diagram of Fig. 1b. The average sea level is chosen to be the reference datum. The first layer in the conceptual model consists of the eroded Quaternary aquifer and the weathered fractured-karst aquifer whose bottom is 50 m below the top boundary, which is the free water table (see Fig. 1a). The second layer primarily consists of a well-developed karst aquifer whose bottom is approximately 80 m b.s.l. (−80 m). The third layer is a poorly developed karst aquifer whose bottom is approximately 160 m b.s.l. (−160 m; Wang and Zhang 1999; Zhu et al. 2000; Li et al. 2003). It is worthwhile to point out that the first layer is regarding vertical variation of the water table, and the bottom of the first layer or the upper boundary of the second layer also has vertically variable topography. The bottoms of the second and third layers are horizontal. However, the horizontal scale of the domain is much greater than the

Table 1 The monthly averaged water table versus time (months) at observation wells 14, 38, and S-51 in years 2001 and 2002

No.	2001											
	1	2	3	4	5	6	7	8	9	10	11	12
14	18.55	19.21	19.60	19.20	17.67	15.90	16.06	16.48	16.06	15.92	15.61	16.30
38	24.44	24.86	24.92	23.08	22.01	21.13	21.83	22.73	23.71	24.02	23.95	23.32
S-51	25.20	25.19	25.04	22.40	21.74	20.10	20.1	22.00	23.00	22.50	23.10	24.55
No.	2002											
	1	2	3	4	5	6	7	8	9	10	11	12
14	16.14	16.49	16.46	14.93	13.78	13.72	12.58	11.49	10.64	10.37	10.21	10.34
38	23.63	23.14	22.81	21.33	19.66	20.56	19.63	17.71	16.34	19.56	17.94	17.99
S-51	23.40	24.40	23.30	22.20	21.20	21.30	20.01	18.50	17.83	19.56	19.45	19.62

The unit is meters and the datum is the average sea level

 DOI 10.1007/s10040-006-0061-0

vertical scale, thus flow is primarily horizontal except at the discharge zones such as springs, rivers, etc.

The boundary conditions for the three layers are shown in Fig. 2. Identical boundary conditions are used for the second and third layers. The southern boundaries for all three layers are the water divide below the Tai Mountain ridge, thus are treated as no-flow boundaries. The eastern and western boundaries for all three layers are along the Wenzu and Mashan faults, respectively. They are also regarded as no-flow boundaries. To the north, the first layer is bounded by the seasonal Xiaoqinghe River, and the second and third layers are mostly bounded by the igneous rocks except the northwestern portion, which is in contact with the Xiaoqinghe River. In theory, a river boundary can be regarded as the third type, or head-dependent flux boundary if there is a less permeable barrier separating the river from the subsurface aquifer. Field observations indicate that the seasonal Xiaoqinghe River is hydraulically well connected with the subsurface aquifer and is better treated as a second kind or flux boundary. The igneous rocks that bound the second and third layers on the north are treated as no-flow boundaries. The top boundary of the first layer is the free water table. The bottom of the third layer is the bedrock, which is treated as a no-flow boundary.

As pointed out by Anderson and Woessner (1992), using the second kind of boundary (flux boundary) exclusively in the groundwater flow model might result in an instability problem. To avoid this, the observation wells at the boundary (such as well Nos. 14, 38, and S-51, which are screened in the second layer) are used as boundary type 1 (see Fig. 3). The monthly averaged water levels versus time for these three wells between 2001 and 2002 are recorded in Table 1.

Finite element method

To solve the flow Eq. (1), the Galerkin finite-element method is employed by dividing the region Ω into hexahedral elements. There are 8 nodes in each hexahedral element. Thus Eq. (1) can be written as

$$\sum_{e=1}^{M}\left\{\begin{array}{l}\iiint_e K_{xx}^e\left(\frac{\partial\widehat{H}}{\partial x}\frac{\partial N_l}{\partial x}+K_{yy}^e\frac{\partial\widehat{H}}{\partial y}\frac{\partial N_l}{\partial y}+K_{zz}^e\frac{\partial\widehat{H}}{\partial z}\frac{\partial N_l}{\partial z}\right)dxdydz \\ +\iiint_e N_l S_s^e\frac{\partial\widehat{H}}{\partial t}dxdydz-\iiint_e N_l W dxdydz-\iint_{S_2^e} N_l q ds\}=0\end{array}\right\},(l=1,2,\cdots,8) \tag{2}$$

where M is the number of elements, l is the number of nodes in an element, N_l is the basis functions, $\widehat{H}$ is the trial function in the element e, and is expressed as

$$\widehat{H}=\sum_{i=1}^{8}H_i N_i, \tag{3}$$

where H_i is the hydraulic head at node i. Substituting Eq. (3) into Eq. (2) leads to the following matrix equation

$$[d]\left\{\widehat{H}\right\}+[p]\left\{\frac{d\widehat{H}}{dt}\right\}=\{f\} \tag{4}$$

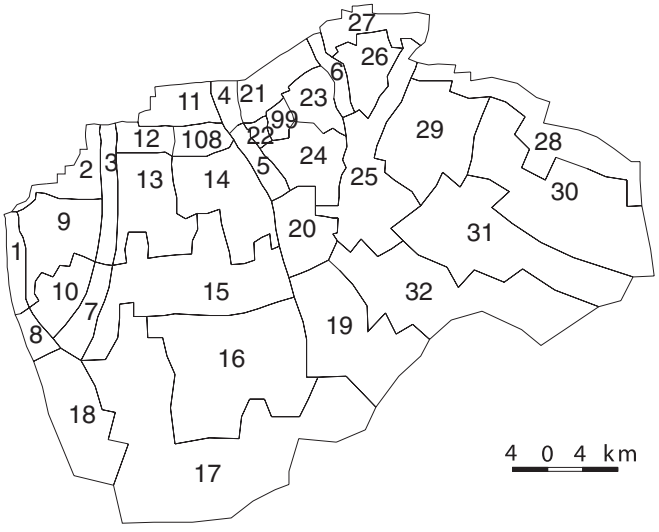

Fig. 4 The hydraulic conductivity and the specific yield zones for the first layer

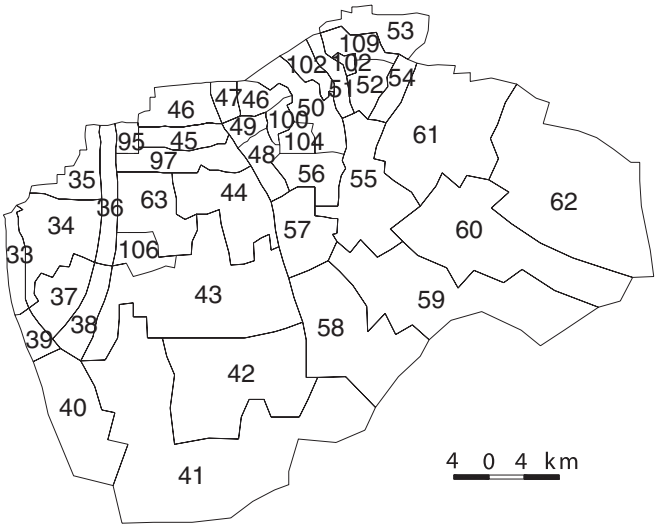

Fig. 5 The hydraulic conductivity and the specific yield zones for the second layer

 DOI 10.1007/s10040-006-0061-0

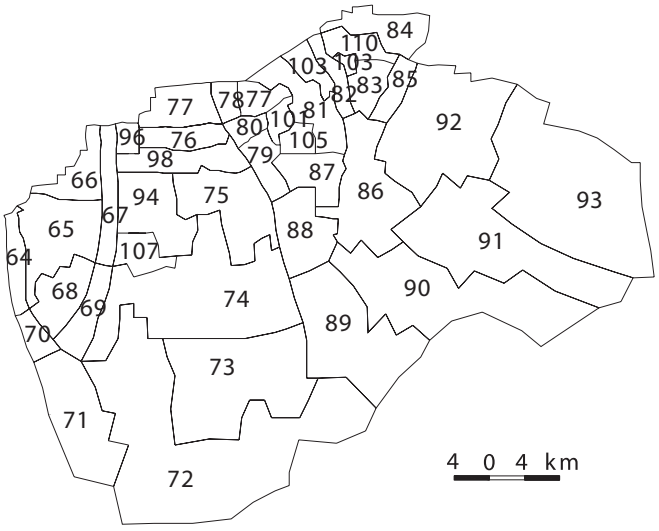

Fig. 6 The hydraulic conductivity and the specific yield zones for the third layer

where

$$d_{il} = \int_e \int\int \left[K^e_{xx} \frac{\partial N_i}{\partial x} \frac{\partial N_l}{\partial x} + K^e_{yy} \frac{\partial N_i}{\partial y} \frac{\partial N_l}{\partial y} + K^e_{zz} \frac{\partial N_i}{\partial z} \frac{\partial N_l}{\partial z} \right] dxdydz, \tag{5}$$

$$p_{il} = \int_e \int\int S^e_s N_i N_l dxdydz, \tag{6}$$

$$f_l = \int_e \int\int W^e N_l dxdydz \tag{7}$$

For a hexahedral element with an irregular shape, it is difficult to solve Eqs. (4), (5), (6), (7). To overcome this difficulty, Pinder and Frind (1972) and Huyakorn and Pinder (1983) have proposed a coordinate transformation that converts the irregular hexahedral element into an equivalent cubic element upon which the finite element method can be easily applied. The basis function for this new set of coordinates (ξ, η, ζ) then becomes

Table 2 The hydraulic conductivity and the specific storage fitted for different zones in the first layer. K_{xx}, K_{yy}, and K_{zz} are the principal hydraulic conductivities along the x, y and z directions, respectively

Layer	No. (see Fig. 4)	Conductivity (m/day)			Specific storage (m^{-1})	Main stratum and faults
		K_{xx}	K_{yy}	K_{zz}		
I	1	1.12	1.36	0.009	0.052	Q Mashan fault
	2	0.065	0.077	0.0004	0.056	Q
	3	0.18	0.31	0.0004	0.036	Q Chaomidian fault
	4	0.39	0.76	0.0009	0.038	Q Qianfoshan fault
	5	0.28	0.49	0.0028	0.055	O Qianfoshan fault
	6	0.78	0.52	0.0036	0.049	Q Ganggou fault
	7	0.021	0.036	0.011	0.038	O Qianfoshan fault
	8	0.40	0.67	0.039	0.053	∈ Mashan fault
	9	0.023	0.035	0.002	0.048	O
	10	0.021	0.026	0.008	0.041	∈
	11	1.02	1.12	0.00005	0.046	Q
	12	1.18	1.26	0.0233	0.058	Q
	13	0.49	0.72	0.0019	0.051	O
	14	2.96	1.86	0.088	0.042	O
	15	1.48	0.58	0.0005	0.061	O
	16	1.38	0.38	0.0003	0.058	∈
	17	0.0011	0.0018	0.0002	0.041	Ar
	18	0.002	0.069	0.001	0.033	Ar
	19	0.12	0.26	0.0001	0.058	O Qianfoshan fault
	20	0.24	0.37	0.16	0.043	∈
	21	2.76	4.38	0.0038	0.038	Q
	22	1.68	1.78	0.0178	0.042	C_{3t}
	23	2.56	4.09	0.058	0.052	C_{3t}
	24	0.75	0.89	0.0196	0.036	C_{3t}
	25	0.76	1.62	0.005	0.044	O Ganggou-Dongwu fault
	26	1.85	2.96	0.0038	0.046	Q
	27	8.58	12.56	0.188	0.052	Q
	28	1.32	1.58	0.16	0.058	Q
	29	1.25	2.79	0.12	0.056	O
	30	1.11	1.24	0.062	0.068	O
	31	0.36	0.22	0.18	0.052	∈
	32	0.08	0.17	0.0178	0.062	Ar
	99	0.10	0.11	0.12	0.04	C_{3t}
	108	3.98	5.06	0.014	0.052	Q

The definition of symbols is as follows. *Q* Quaternary, ∈ Cambrian, *O* Ordovician, γ igneous rock, *Ar* Archaean layer, *C* Carboniferous. Subscripts 2 and 3 represent middle and late epochs. Subscripts t, f, and z represent Taiyuan, Fengshan, and Zhangxia groups, respectively

 DOI 10.1007/s10040-006-0061-0

$$N_i(\xi,\eta,\zeta)=\frac{1}{8}(1+\xi\xi_i)(1+\eta\eta_i)(1+\zeta\zeta_i) \quad (8)$$

A detailed explanation of the coordinate transformation can be found from Pinder and Frind (1972) and Huyakorn and Pinder (1983) and will not be repeated here. The finite-element program for this study is primarily developed at the Hefei University of Technology in China.

Discretization of the domain

The study domain is discretized using hexahedron elements for each layer. Discretization is identical for all three layers. The mesh design for the second layer is shown in Fig. 3 where the black dots represent the observation wells screened at that layer. The total number of elements is 3,294, and the total number of nodes is 4,680.

The parameters are identified by the zonation method which has been described in details by Yeh (1986). In this method, the flow region is divided into a number of sub-regions, or zones based on the fractured-karst characteristics, and the tectonics and other geological characteristics of the site. The hydraulic parameters are uniform across a particular zone. The map of zones for the first, the second, and the third layers are shown in Figs. 4, 5 and 6, respectively. The corresponding simulated hydraulic conductivity and specific storage values are presented in Tables 2, 3, 4, respectively.

Infiltration and evapotranspiration

It is well recognized among hydrologists that a precise measurement of groundwater recharge over a large natural flow system is still a challenging task (Scanlon et al. 2002). In this study, the historic data of precipitation and the surface evapotranspiration rate of the studied region are available. The percentages of the precipitation and evapotranspiration that eventually become groundwater recharge and discharge are classified by the recharge and evapotranspiration coefficients, respectively. Therefore,

Table 3 The hydraulic conductivity and the specific storage fitted for different zones in the second layer

Layer	No. (see Fig. 5)	Conductivity (m/day)			Specific storage (m^{-1})	Main stratum and faults
		K_{xx}	K_{yy}	K_{zz}		
II	33	0.88	1.18	0.16	0.0003	ϵ_{3f}-O Mashan fault
	34	3.08	4.16	0.19	0.00004	ϵ_{3f}-O
	35	2.29	3.41	0.07	0.0003	ϵ_{3f}-O
	36	1.8	3.8	0.04	0.00009	O_2 Chaomidian fault
	37	3.2	3.06	0.96	0.00026	ϵ_2
	38	0.52	4.56	1.95	0.00009	ϵ_2 Chaomidian fault
	39	0.58	0.18	0.066	0.0003	ϵ_2 Mashan fault
	40	0.031	0.22	0.025	0.0003	ϵ_2 Mashan fault
	41	1.41	0.81	0.62	0.00009	Ar
	42	3.28	1.23	0.88	0.0003	Ar
	43	2.59	0.68	0.32	0.00009	ϵ_{2z}
	44	0.79	1.8	0.59	0.0001	O
	45	86.8	70.6	4.6	0.0002	O
	46	0.0001	0.0001	0.0001	0.00001	γ
	47	0.88	2.16	1.05	0.0003	γ Qianfoshan fault
	48	3.06	15.8	2.19	0.0001	ϵ_3-O Qianfoshan fault
	49	258.0	299.0	4.68	0.000018	ϵ_3-O Springs location
	50	12.8	18.8	3.20	0.0002	ϵ_3-O
	51	2.50	8.80	2.25	0.0005	O Dongwu fault
	52	12.8	10.8	1.23	0.00009	O
	53	38.0	49.3	3.18	0.0003	C
	54	60.4	104.6	10.8	0.0005	O Ganggou fault
	55	15.6	25.2	3.36	0.0004	ϵ_3-O Ganggou fault
	56	4.8	6.8	2.28	0.0005	ϵ_3-O
	57	4.48	4.96	1.96	0.0002	ϵ_3-O Qianfoshan fault
	58	4.16	5.38	2.36	0.0001	Ar
	59	1.65	3.77	0.84	0.0003	Ar
	60	25.6	20.4	6.20	0.0003	ϵ_2
	61	8.8	9.3	1.8	0.00006	O
	62	27.7	28.8	2.40	0.0002	O
	63	2.90	3.80	0.86	0.0001	O
	95	38.7	42.8	4.20	0.0006	O
	97	20.8	26.2	2.08	0.0004	O
	100	8.80	10.9	2.40	0.00003	ϵ_3-O
	102	0.35	5.0	2.60	0.0004	γ
	104	16.8	22.8	1.33	0.000012	ϵ_3-O
	106	3.80	4.80	2.30	0.00005	ϵ_2
	109	48.8	47.9	5.80	0.00003	O

The definition of symbols is as follows. *Q* Quaternary, ϵ Cambrian, *O* Ordovician, γ igneous rock, *Ar* Archaean layer, *C* Carboniferous. Subscripts 2 and 3 represent middle and late epochs. Subscripts t, f, and z represent Taiyuan, Fengshan, and Zhangxia groups, respectively

 DOI 10.1007/s10040-006-0061-0

Table 4 The hydraulic conductivity and the specific storage fitted for different zones in the third layer

Layer	No. (see Fig. 6)	Conductivity (m/day)			Specific storage (m^{-1})	Main stratum and faults
		K_{xx}	K_{yy}	K_{zz}		
III	64	0.38	1.08	0.19	0.00007	$\in_{3f}$-O Mashan fault
	65	1.96	1.72	0.77	0.0005	$\in_{3f}$-O
	66	2.19	2.16	0.98	0.0003	$\in_{3f}$-O
	67	1.6	5.20	0.018	0.00008	O2 Chaomidian fault
	68	3.60	4.80	0.72	0.0004	$\in_2$
	69	0.39	3.56	1.52	0.0004	$\in_2$ Chaomidian fault
	70	0.23	0.095	0.021	0.00008	$\in_2$ Mashan fault
	71	0.028	0.059	0.018	0.0003	$\in_2$ Mashan fault
	72	0.32	0.69	0.18	0.0003	Ar
	73	2.06	1.53	0.41	0.0004	Ar
	74	1.70	0.59	0.40	0.0008	$\in_{2z}$
	75	0.63	1.08	0.026	.0002	O
	76	73.8	63.6	2.55	0.0002	O
	77	0.105	0.088	0.031	0.0001	γ
	78	1.02	3.52	0.021	0.0005	γ Qianfoshan fault
	79	1.95	12.8	1.70	0.0002	$\in_3$-O Qianfoshan fault
	80	228.0	252.0	1.88	0.000024	$\in_3$-O Spring field
	81	10.6	15.8	2.20	0.0003	$\in_3$-O
	82	1.60	6.80	1.78	0.00006	O Dongwu fault
	83	1.80	2.80	0.58	0.00008	O
	84	36.8	37.5	2.87	0.0005	C
	85	56.6	97.6	10.8	0.0006	O Ganggou fault
	86	14.8	23.6	3.24	0.0003	$\in_3$-O Ganggou-Dongwu fault
	873.80	5.90	0.077	0.0004	$\in$3–O	
	88	1.86	3.26	1.24	0.0002	$\in_3$-O Qianfoshan fault
	89	2.58	3.66	1.58	0.0001	Ar
	90	1.46	1.70	0.80	0.00032	Ar
	91	20.1	21.6	1.95	0.0003	$\in_2$
	92	5.8	8.80	1.20	0.00005	O
	93	28.6	24.9	1.42	0.0002	O
	94	1.32	2.63	0.09	0.0004	O
	96	33.8	38.6	4.88	0.0004	O
	98	18.2	17.6	1.86	0.0003	O
	101	6.80	8.50	1.80	0.0002	$\in_3$-O
	103	0.26	4.20	1.80	0.0003	γ
	105	15.6	18.6	1.07	0.000013	$\in_3$-O
	107	2.80	3.90	1.50	0.00006	$\in_2$
	110	38.6	47.9	3.68	0.0002	O

The definition of symbols is as follows. *Q* Quaternary, $\in$ Cambrian, *O* Ordovician, γ igneous rock, *Ar* Archaean layer, *C* Carboniferous. Subscripts 2 and 3 represent middle and late epochs. Subscripts t, f, and z represent Taiyuan, Fengshan, and Zhangxia groups, respectively

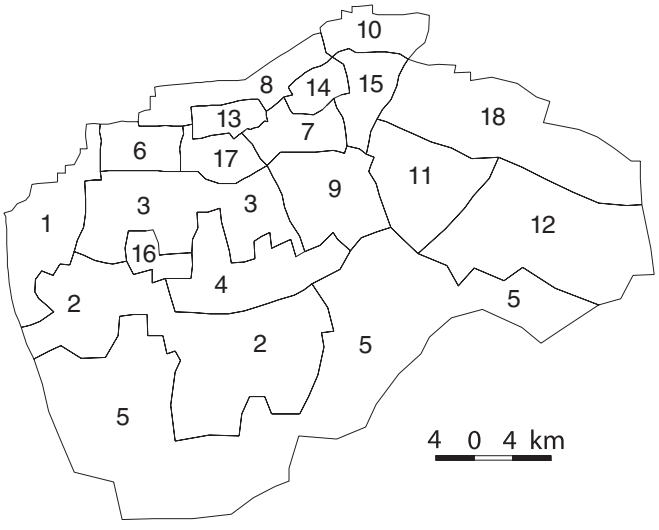

Fig. 7 The zones of different recharge and evapotranspiration coefficients

the actual recharge rate is the product of the precipitation and the recharge coefficient, and the actual evapotranspiration rate is the product of the surface evapotranspiration rate and the evapotranspiration coefficient. The map of zones of recharge and evapotranspiration coefficients is shown in Fig. 7 based on the pattern of precipitation distribution, geographic features, rock types, surface vegetation, etc. The corresponding simulated recharge and evapotranspiration coefficients are shown in Table 5.

Parameter identification and calibration

The hydraulic conductivities and the specific storage as shown in Tables 2, 3, 4 and the recharge and evapotranspiration coefficients shown in Table 5 are determined by an optimization procedure using the following objective function

$$E = \sum_{i=1}^{M} \sum_{j=1}^{N} W_j \left(H_{ij}^c - H_{ij}^0 \right)^2 \tag{9}$$

 DOI 10.1007/s10040-006-0061-0

Table 5 The simulated recharge and evapotranspiration coefficients for the Jinan Springs field

Zone No. (see Fig. 7)	Recharge coefficient	Evapotranspiration coefficient
1	0.27	0.19
2	0.19	NE
3	0.21	NE
4	0.29	NE
5	0.26	NE
6	0.25	0.023
7	0.26	NE
8	0.27	0.24
9	0.32	NE
10	0.21	0.023
11	0.38	NE
12	0.31	NE
13	0.09	NE
14	0.33	0.0088
15	0.31	NE
16	0.38	NE
17	0.22	0.0088
18	0.32	0.023

NE negligible evapotranspiration rate where the water table is deep enough

where M and N are the total numbers of time periods and observation wells, respectively, W_j is a weight function which is commonly set to be unity, implying that all the data points are equally important (Yeh 1986). While the equal value of weight function might not always be the best choice for the optimization of the parameter identification, the required additional information for choosing different weight functions is often not available. Thus, for the sake of simplicity, an equal weight function of unity is used in this study. H_{ij}^{c} is the calculated head, i and j are the indexes of time periods and observation wells, respectively, and H_{ij}^{0} is the measured head. Parameters are adjusted to minimize the objective function E.

The optimization procedure used in this study is briefly described as follows. The weight function W_j is set to be 1. The absolute values of the difference and the relative difference between the measured and simulated heads, denoted as $\left|H_{ij}^{c}-H_{ij}^{0}\right|$ and $\left|H_{ij}^{c}-H_{ij}^{0}\right|/H_{ij}^{0}$, respectively, are checked according to the standard GB/T14497-93 as implemented by the Ministry of Land and Resources of China. According to this standard, the number of nodes with $\left|H_{ij}^{c}-H_{ij}^{0}\right|/H_{ij}^{0}$ less than 10% should at least be 70% of the total nodes. In addition to this requirement, at the regions with relatively small drawdowns, the number of nodes with $\left|H_{ij}^{c}-H_{ij}^{0}\right|$ less than 0.5 m should at least be 70% of the nodes of those regions.

The total number of observation wells used is 35. Of these, 9 wells are screened in the first layer, 24 wells are screened in the second layer with three of them used as the first type of boundary condition (see Fig. 3), and two wells

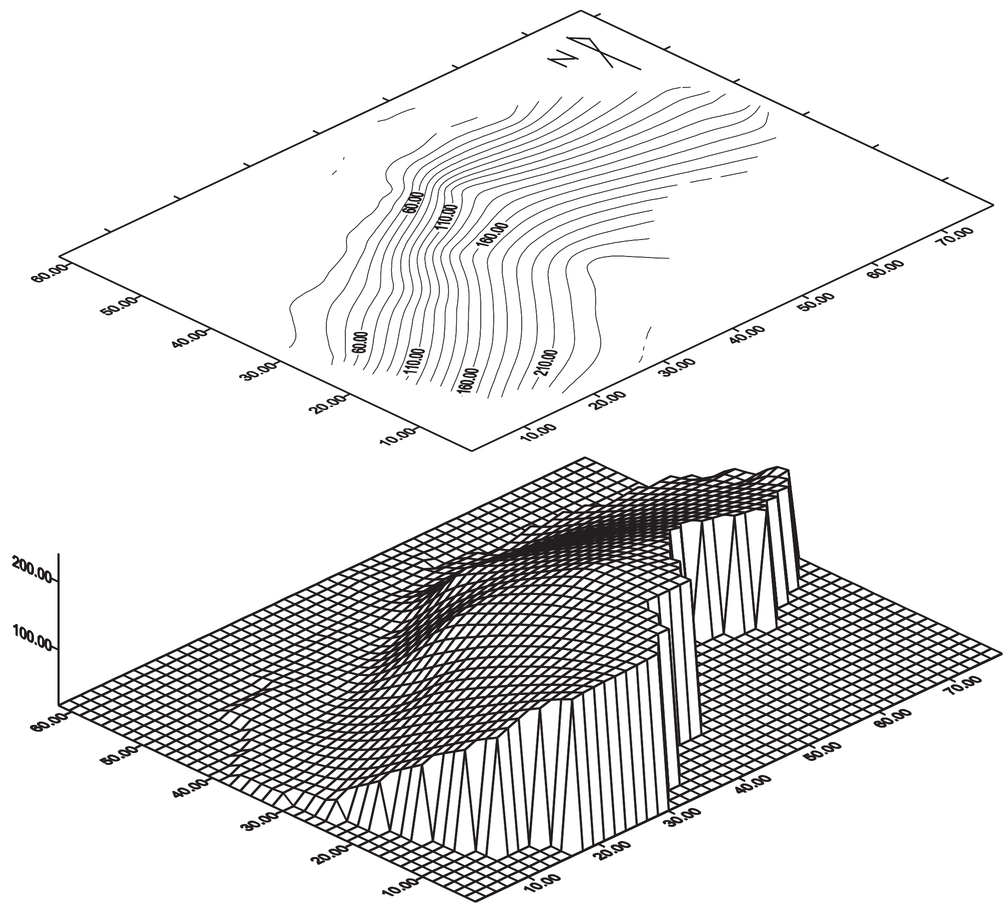

Fig. 8 The contour and surface maps of the initial groundwater hydraulic heads for all three layers (1 January 2001). The scales are in meters

DOI 10.1007/s10040-006-0061-0

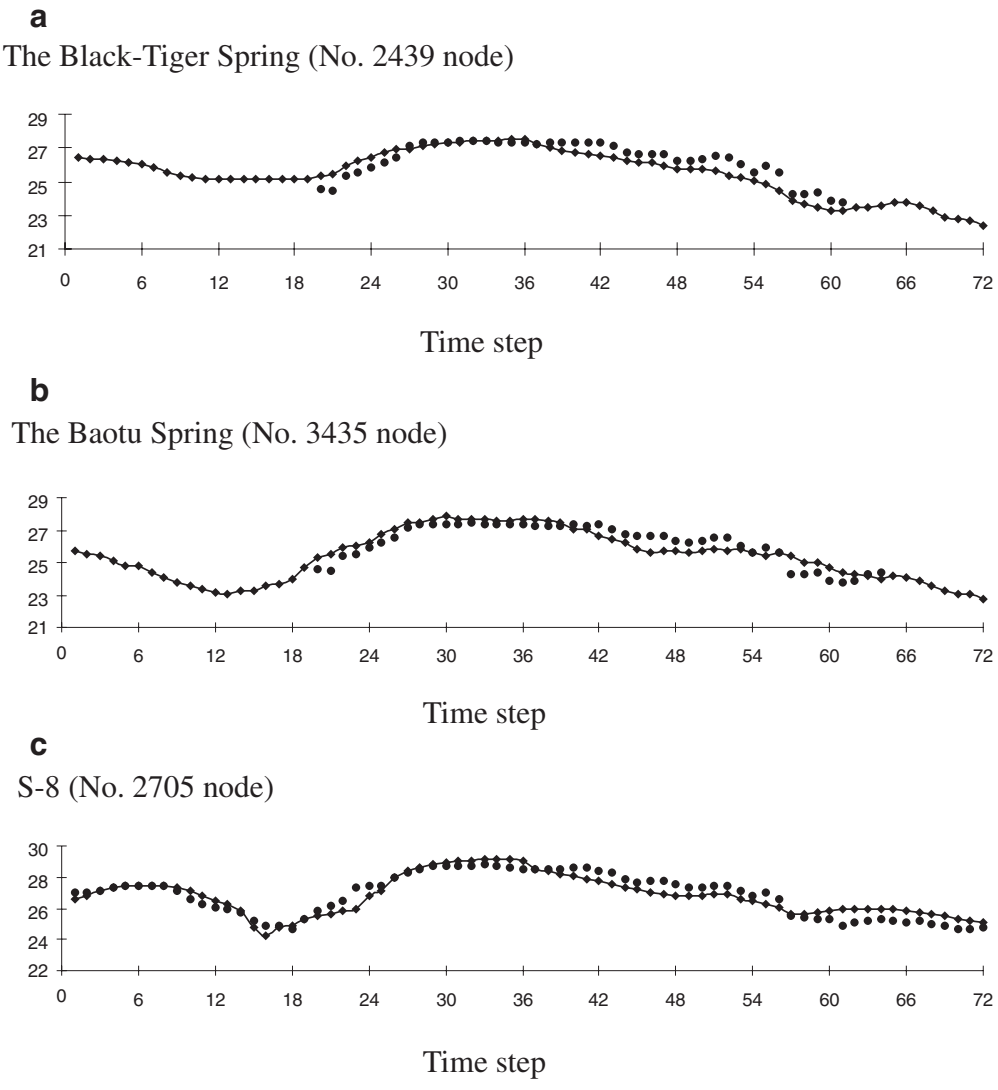

Fig. 9 Comparison of the calculated versus the observed hydraulic heads at **a** the Black-Tiger Spring (No. 2439 node), **b** the Baotu Spring (No. 3435 node), and **c** well S-8 (No. 2705 node). The *black dots* represent the measured head and the *diamonds* represent the calculated head. The vertical axes scales are meters above sea level. Each time step is 10 days

are screened in the third layer. The locations of the wells screened in the second layer are shown in Fig. 3. Among the 32 observation wells (excluding the 3 wells used as the boundary condition), 23 of them are used for observing hydraulic head in the karst, and the rest (9) are used for observing hydraulic head in the porous media.

The optimization process yields the best-fit parameters of the hydraulic conductivity and the specific storage of each zone and the recharge coefficients of the 18 designated recharge zones, and the evapotranspiration coefficients of 7 of those recharge zones. The water tables in the remaining (11) recharge zones are sufficiently deep to eliminate the evapotranspiration (see Table 5). The simulated parameters are checked with other 'soft' information such as precipitation distribution, geographic and geological features, rock types, surface vegetation, etc. Nevertheless, non-uniqueness of the simulated parameters is possible. With further information gained through direct measurement of the hydraulic conductivities and the specific storage, probably via pumping tests, and measurements of the recharge and evapotranspiration rates at certain zones, additional constraints can be put on the

Table 6 The average and maximum absolute differences at the period of parameter identification (Jan. to Dec. 2001) and the period of calibration (Jan. to Dec. 2002) at the Black-Tiger Spring (No. 2439 node), the Baotu Spring (No. 3435 node), and well S-8 (No. 2705 node)

Nodes No.	Period of parameter identification (Jan. to Dec. 2001)		Period of calibration (Jan. to Dec. 2002)	
	Average absolute difference (m)	Maximum absolute difference (m)	Average absolute difference (m)	Maximum absolute difference (m)
2439	0.33	0.97	0.62	1.10
2435	0.40	0.96	0.54	1.17
2705	0.31	1.38	0.56	1.03

 DOI 10.1007/s10040-006-0061-0

choice of those parameters, and a better optimization might be achieved.

The model parameters are identified in a two-step process. First, the groundwater head distribution of January of 2001, as shown in Fig. 8, is used as the initial condition of the simulation. The groundwater head distribution in December of 2001 is used for preliminary parameter identification. Second, the preliminarily identified parameters in 2001 are then refined by calibrating the simulated hydraulic heads with the measured heads in December of 2002. The year of 2001 is termed the parameter identification period and the year of 2002 is the calibration period.

The duration between the starting time of the simulation and the calibration is relatively short. Ideally, the data of groundwater head distribution from multiple years is be better for calibrating the model. However, several considerations and practical limitations lead to this choice. First, a reliable database of hydraulic head distribution before 2001 is unfortunately not available. Second, there was a large artificial recharge event along the Yufuhe River from Wohushan Reservoir, from 18 August 2001 to 4 September 2001 with a total recharge volume of 8.0×10^6 m^3. This recharge event occurred within a relatively short period of time and acted like a transient stress or disturbance, imposing on the hydrologic system. Such a stress will propagate through the aquifer system and its signal might be detected by changes in hydraulic head in the observation wells that are sufficiently close to the source of this recharge event. It is notable that this recharge event happened at the southwestern side of the research domain (see Fig. 1) and the three observation points that are used as the first type of boundary condition are located at the northeastern side of the domain (see Fig. 3 and Table 1), thus the influence of this recharge event on the change of water levels at those three observation points (14, 38 and S-51) is not significant.

Each time step is 10 days, and there are 72 time steps covering 2 years from January 2001 to December 2002. Simulation results show that 78.1% of the observation wells have less than 10% differences between the measured and the computed heads in the first year. During the calibration period (the second year), 72.4% of the observation wells have less than 10% differences between the measured and the computed heads. In particular, for the Black-Tiger Spring and the Baotu Spring, the time periods in which the absolute differences between the measured and the computed hydraulic heads are less than 0.5 m are 80.6 and 77.8% of the entire simulation periods (2 years), respectively.

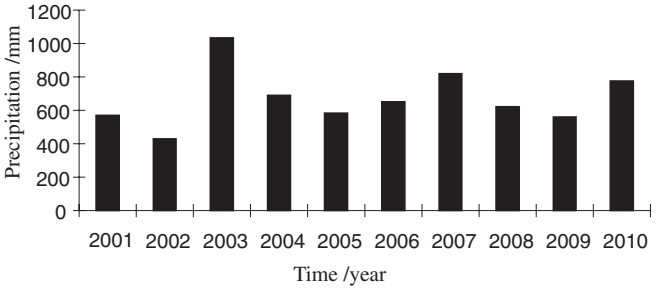

Fig. 10 The total annual amount of precipitation predicted in the Jinan Springs field from 2003 to 2010

Figure 9 shows the head differences between the measured and the computed values at the Black-Tiger Spring (No. 2439 node), the Baotu Spring (No. 3435 node), and the well S-8 (No. 2705 node). The agreement between the measured and the computed values appears to be satisfactory. Table 6 shows the average absolute difference and the maximum absolute difference between the measured and the computed hydraulic heads at the Black-Tiger Spring (No. 2439 node), the Baotu Spring (No. 3435 node), and the well S-8 (No. 2705 node). During the period of parameter identification (January to December 2001), the average absolute differences are less than 0.5 m and the maximum absolute differences are around 1.0 m. For the calibration period (January to December 2002), the average absolute differences are slightly greater than 0.5 m, and the maximum absolute differences are slightly greater than 1.0 m.

The mass balances of the simulation for year 2001 and 2002 are summarized in Table 7 in which the recharge terms (1)–(4) represent the vertical recharge from precipitation, the lateral recharge from the flux boundary condition, the recharge from surface water bodies, and the vertical recharge from the unconsolidated Quaternary layer, respectively; and the discharge terms (5) and (6) represent the pumping and the natural discharge, respectively. It is notable that the total recharge budget is slightly greater than the total discharge budget in 2001, resulting in a small positive storage budget. This result is also reflected in the slight increase in water levels at the Black-Tiger Spring, the Baotu Spring, and the well S-8 in Fig. 9 where time steps 0–36 are for 2001. The total recharge budget is less than the total discharge budget in 2002, as reflected in the negative storage budget (depletion) in Table 7. This

Table 7 The mass balance of simulation in 2001–2002 in cubic meters (m^3)

Year	I: Recharge=(1)+(2)+(3)+(4)				II: Discharge=(5)+(6)		I–II Balance
	(1)	(2)	(3)	(4)	(5)	(6)	
2001	287,786,900	14,899,800	13,654,000	1,214,400	245,363,500	72,170,000	21,600
2002	207,862,380	15,866,400	8,621,000	892,600	201,741,000	40,836,000	−934,620

Recharge terms: *(1)* vertical recharge from precipitation, *(2)* lateral recharge from the flux boundary condition, *(3)* recharge from surface water bodies, *(4)* vertical recharge from the unconsolidated Quaternary layer, respectively. Discharge terms: *(5)* pumping, *(6)* natural discharge

 DOI 10.1007/s10040-006-0061-0

Table 8 Three schemes of fractured-karst aquifer exploitation

Schemes	Exploitation of fracture-karst water in different zones($\times10^4$ m^3/day)				Sum ($\times10^4$ m^3/day)
	Between Mashan fault and Qianfoshan fault	Between Qianfoshan fault and Dongwu fault	Between Dongwu fault and Ganggou fault	Between Ganggou fault and the east border	
I	25.43	21.29	21.14	1.51	69.37
II	21.55	15.09	22.62	1.53	60.79
III	8.46	5.1	11.84	1.53	26.96[a]

[a]Adding surface water supply: 90×10^4 m^3/day, as well as reuse water supply 20×10^4 m^3/day for the city of Jinan

result is also supported by the decline of water levels at the Black-Tiger Spring, the Baotu Spring, and the well S-8 in Fig. 9 where time steps 37–72 are for 2002.

The fitted hydraulic conductivities and the specific storages are given in Tables 2, 3, 4 and the fitted recharge and evapotranspiration coefficients are given in Table 5. Notice that three principal hydraulic conductivities are used for each zone in Tables 2, 3, 4, thus anisotropy is considered. The values of fitted hydraulic conductivities and the specific storages agree with the field observation of the sediment and rock types.

Application of the numerical simulation for spring protection

Prediction of precipitation

Precipitation accounts for a large percentage of the groundwater recharge, thus the precipitation in the future will directly affect the result of the model. In this study, a non-stationary self-regressive model is employed to predict the precipitation values from 2003 to 2010 based on the precipitation per month from 1994 to 2002 (Tong and Lim 1980). The result is shown in Fig. 10. The product of the precipitation and the calibrated recharge coefficient in Table 6 is approximated as the predicted recharge; whereas the evapotranspiration is expected to be similar to what has been used in 2001 and 2002 (see Table 5).

Schemes of groundwater exploitation and spring protection

In this study, the hydraulic heads of the Baotu Spring (at an elevation of 26.80 m a.s.l.) and the Black-Tiger Spring (at an elevation of 27.50 m a.s.l.) are respectively selected as the control criterions. Three schemes with progressively decreasing groundwater exploitation rates are investigated and the details of the schemes are listed in Table 8. The rate of the first scheme (I), 69.37×10^4 m^3/day, represents present groundwater exploitation. The deficit of water demand of the city and the amount of groundwater withdrawal will be met by the available surface water and recycled waste water in the area.

In Fig. 11, the hydraulic heads versus time for three schemes of water exploitation are compared. Under the condition of scheme I, the Baotu Spring will become dry for several short periods of time during 2004–2010, while the Black-Tiger Spring will become dry for some significant periods of time almost every year. Obviously, exploitation by this scheme is less favorable in terms of spring protection, particularly the protection of the Black-Tiger Spring. Compared to scheme I, scheme II decreases the fractured-karst water exploitation from 69.37×10^4 to

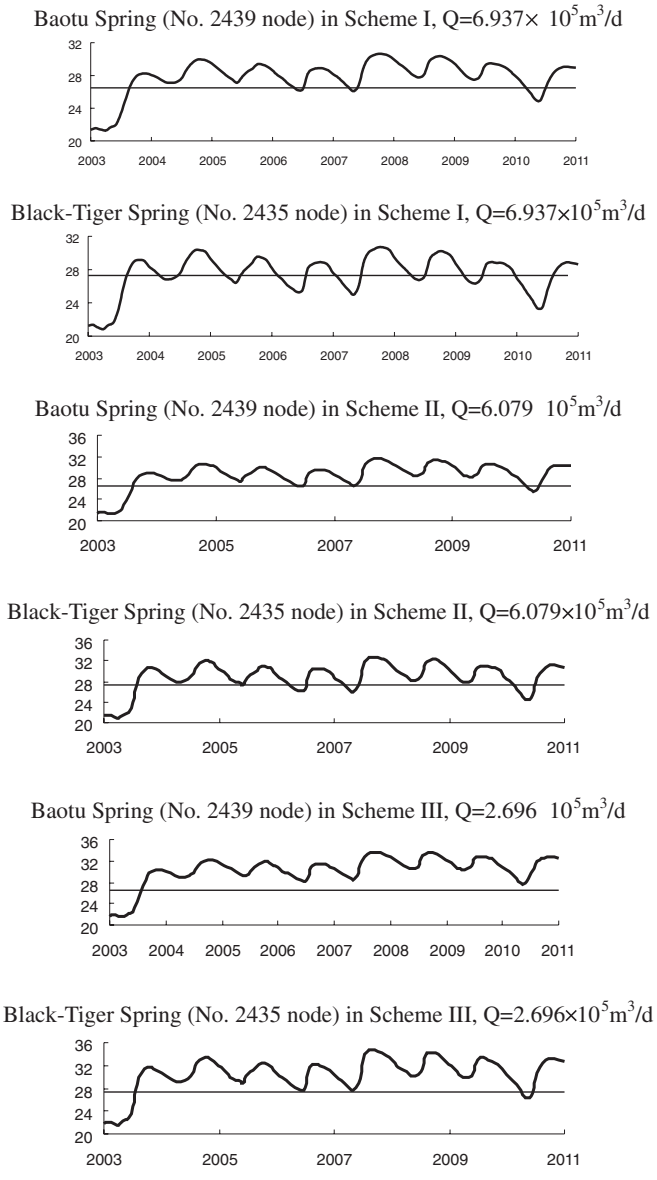

Fig. 11 The hydraulic heads at the Baotu and the Black-Tiger springs under various exploitation plans. The scales of the vertical axes are meters above sea level

 DOI 10.1007/s10040-006-0061-0

60.79×10^4 m^3/day (shown in Table 8) and the groundwater levels slightly rise, but there are still some considerable periods of time during which the Black-Tiger Spring becomes dry. The durations of the dry period are shorter than that in scheme I.

In the third scheme (III), groundwater exploitation is substantially decreased to 26.96×10^4 m^3/day. This amount is chosen by considering the available surface water supply in the region, which has a capacity of 90×10^4 m^3/day, and the recycled waste water supply with the capacity of 20×10^4 m^3/day. Because of the reduction of groundwater pumpage in scheme III, the groundwater level of the Baotu Spring is higher than the control criterion, while the same is true for the Black-Tiger Spring in the following years except a short period of time in 2010. In conclusion, the simulations conducted in this work suggest that only scheme III would protect the spring flow in the city of Jinan.

Discussion and conclusion

A three-dimensional finite-element model is developed to simulate groundwater flow in a large fractured-karst system in Jinan Springs field and agreement is made among the simulated and observed hydraulic heads in 32 observation wells. Various schemes of groundwater exploitation for spring protection have been put forward and their respective effects on the table are analyzed and compared. Finally, an optimal strategy for spring protection is suggested.

It is pointed out that the spring protection plan proposed as a result of this study is based on a few presumptions. For instance, the amount of groundwater exploitation is based on present prediction of water demands of the city of Jinan and the availability of the surface and recycled water to 2010. The numerical simulation is based on an EPMM approach to approximate groundwater flow in the fractured-karst aquifers. If any of those presumptions are altered during the predicted period, the model should be revised accordingly. In conclusion, this study shows that the scheme III in which the amount of groundwater exploitation is set up to be 26.96×10^4 m^3/day might be an adequate plan for protecting the precious Jinan Springs field.

Acknowledgements The research was supported by the National Natural Science Foundation of China (No. 40202027) and Fok Ying Tung Education Foundation (No. 91079). We thank Associate Editor Mary Hill for her detailed comments which helped us greatly in revising the manuscript. We also thank another reviewer Laura Foglia for her constructive comments and Sue Duncan (Technical Editorial Advisor) for further editorial corrections.

References

Anderson MP, Woessner WW (1992) Applied groundwater modeling. Academic Press, San Diego, USA

Birk S, Liedl R, Sauter M (2004) Identification of localised recharge and conduit flow by combined analysis of hydraulic and physico-chemical spring responses (Urenbrunnen, SW-Germany). J Hydrol 286:179–193

Chen HH, Zhang YX (2001) Karst reservoir and the surface reservoir in the area in North China (in Chinese). Earth Sci Front 8(1):185–190

Crouch DP (1996) Environmental geology of ancient Greek cities. Environ Geol 27(3):233–245

Elhatip H, Gunay G (1998) Karst hydrogeology of the Kas-Kalkan Springs along the Mediterranean coast of Turkey. Environ Geol 36(1–2):150–158

Huyakorn PS, Pinder GF (1983) Computational methods in subsurface flow. Academic Press, San Diego, USA

Jaquet O, Siegel P, Klubertanz G, Benabderrhamane H (2004) Stochastic discrete model of karstic networks. Adv Water Resour 27(7):751–760

Josnin JY, Pistre S, Drogue C (2000) Modeling of the complex karstic system in Saint-Chaptes (Gard, France): a tool for the synthesis of geological and hydrogeological data. Can J Earth Sci 37(10):1425–1445

Kattan Z (1997) Environmental isotope study of the major karst springs in Damascus limestone aquifer systems: case of the Figeh and Barada Springs. J Hydrol 193:161–182, 1–182

Kaufmann G (2003) A model comparison of karst aquifer evolution for different matrix-flow formulations. J Hydrol 283:281–289

Kaufmann G, Braun J (2000) Karst aquifer evolution in fractured porous rocks. Water Resour Res 36(6):1381–1391

Labat D, Mangin A, Ababou R (2002) Rainfall-runoff relations for karstic springs: multifractal analyses. J Hydrol 256(3–4):176–195

Larocque M, Banton O, Ackerer P, Razack M (1999) Determining karst transmissivities with inverse modeling and an equivalent porous media. Ground Water 37(6):897–903

Li FL, Qian JZ, Wang JQ, Wu YF, Chen XQ (2003) Temporal change of Jinan Springs discharge and protection of the springs. In: Wang YX (ed) Proc International Symposium on Water Resources and the Urban Environment, October 2003, Wuhan, P.R. China, pp 394–396

Oraseanu I, Mather J (2000) Karst hydrogeology and origin of thermal waters in the Codru Moma Mountains, Romania. Hydrogeol J 8(4):379–389

Pinder GF, Frind ED (1972) Application of Galerkin's procedure to aquifer analysis. Water Resour Res 8(1):108–120

Qian JZ, Wu JF, Dong HX, Zhu XY (2003) An isoparametric finite element 3-D numerical model for the fracture-karst flow in a wells field (in Chinese). J Hydraul Eng 3:37–41

Raeisi E, Karami G (1996) The governing factors of the physicochemical characteristics of Sheshpeer Karst Springs, Iran. Carbon Evapor 11(2):162–168

Sauro U (1993) Human impact on the karst of the Venetian forealps, Italy. Environ Geol 21(3):115–121

Scanlon BR, Healy RW, Cook PG (2002) Choosing appropriate techniques for quantifying groundwater recharge. Hydrogeol J 10(1):18–39

Scanlon BR, Mace RE, Barrett ME, Smith B (2003) Can we simulate regional groundwater flow in a karst system using equivalent porous media models? Case study, Barton Springs Edwards aquifer, USA. J Hydrol 276:137–158

Tong H, Lim KS (1980) Threshold auto-regressive limit cycles and cyclical data. J R Stat Soc Ser B 42(3):245–292

Wang GL, Zhang WG (1999) Research on management model for Jinan fissure-karst water system (in Chinese). J Dalian Univ Tech (5):689–693

Wu JF, Zhu XY, Liu JL (1999) Using genetic algorithm based simulated annealing penalty function to solve groundwater management model. Sci China (Series E) 42(5):521–529

Yeh G-T (1986) Review of parameter identification procedures in groundwater hydrology: the inverse problem. Water Resour Res 22(1):95–108

Zhu XY, Liu JL, Zhu JJ (2000) Characteristics of distribution and transport of petroleum contaminants in fracture-karst water in Zibo Area, Shandong Province, China. Sci China (Series D) 43 (2):141–150

 DOI 10.1007/s10040-006-0061-0